In Vivo ^{31}P Magnetic Resonance Spectroscopy Using a Needle Microcoil

Franklyn A. Howe,[1*] Richard R.A. Syms,[2] Munir M. Ahmad,[2] Loreta M. Rodrigues,[3] John R. Griffiths,[3] and Ian R. Young[2]

Batch fabrication methods have been used to produce low-cost microcoils for magnetic resonance spectroscopy (MRS) that could be discarded after applications such as insertion into tissue during interventional surgery. Needle-shaped microcoils were constructed using electroplated conductors buried in shafts formed with different combinations of silicon and plastic and used to acquire in vivo ^{31}P spectra of rat thigh muscle at 81 MHz. The designs in this study achieved a maximum signal-to-noise ratio (SNR) for phosphocreatine (PCr) of 10.4 in a 10-min acquisition, with the three adenosine triphosphate (ATP) multiplets also clearly visible. An average 20% reduction in PCr occurred over a 60-min period, and intracellular pH was estimated to be 6.6, which are both evidence of ischemia. A needle microcoil design could have applications in real-time MRS of tumors or in evaluating pathology in general during surgical investigations. Magn Reson Med 61:1238–1241, 2009. © 2009 Wiley-Liss, Inc.

Key words: ^{31}P magnetic resonance spectroscopy; microcoil; magnetic resonance imaging; muscle; batch fabrication

Planar microcoils based on metallic conductors on a variety of substrates including GaAs (1), Si (2), glass (3), and plastic (4) have been investigated over the past few years. Probes designed for insertion into the body have also been formed, by winding a wire solenoid around the outside of a glass capillary tube (5). The overall aim of this work has been to develop local coils for clinical magnetic resonance spectroscopy (MRS) that could be batch-fabricated at sufficiently low cost that they might be discarded after a single use.

We have been developing an alternative planar design for insertion into tissue, based on a pair of conductors running parallel to the axis of a long, thin needle (6,7) as shown in Fig. 1. Such coils have a very small field of view orthogonal to the longitudinal coil axis and the two conductors have a quadrupolar H-field as shown in Fig. 1a. A coil of such design immersed in a uniform medium would yield little signal in receive-only mode due to signal cancellation from the regions of opposite polarity. The needle coil design actually implemented encloses the conductors with a rectangular block of solid resistive material to eliminate a significant proportion of the signals from one pair of the regions with the same polarity, but is also suitable for use in transmit/receive mode as used in this current study. Considerable improvements have now been made to high-frequency performance, by slowly increasing the thickness of properly insulating material beneath the coil and removing all high-resistivity silicon, improving the unloaded Q-factor and extending the operating frequency from 63.8 MHz to 400 MHz. These changes have involved significant alterations to the fabrication process and have inexorably relegated the role of the silicon substrate to that of a temporary carrier wafer.

To assess the practicality of performing in vivo MRS with such a microcoil design we have acquired data from normal rat thigh muscle. This experiment has the advantages of a large tissue mass for insertion of the coil and a well-known spectroscopic profile. Magnetic resonance imaging (MRI) and MRS measurements were first performed in phantoms to assess the coil sensitivity profile and its pulse power calibration. A needle microcoil tuned to 200 MHz was used for assessment by ^{1}H MRI and coils tuned to 81 MHz were used for ^{31}P MRS measurements.

MATERIALS AND METHODS

Coil Fabrication

Coils were made using planar processes that allowed 100 needles to be manufactured from a 100-mm-diameter silicon wafer. Two variants were assessed. The first were silicon/plastic hybrids (6), in which the lower half of the structure was formed in 550-μm-thick layers of high-resistivity Si and the upper half in a photopatternable epoxy resist, SU-8 (8). The second were needles in which both halves of the shaft were formed in SU-8 (7). This design has improved high-frequency performance due to the elimination of substrate losses immediately adjacent to the windings. Furthermore, a completely plastic design has structural properties that make it more compatible with clinical use than a partly silicon-based design, due to the elimination of brittle crystalline material.

In each case, the needle shaft contained a single-turn coil, based on a pair of conductors that ran parallel at a separation of 1 mm for a distance of 10 mm and then converged together to meet at a tip a further 2.5 mm away. The conductors were 150-μm-wide tracks consisting of 14 μm of copper and 4 μm of gold, electroplated inside a photoresist mould. The conductors were encased in material patterned into a needle outline 200 μm wider than the coil, except at the base. In this region, the outline was expanded further to allow landing sites for nonmagnetic tuning and matching capacitors (Type HighQ, Size 0805;

[1]Division of Cardiac and Vascular Sciences, St George's Hospital, University of London, London, UK.

[2]Department of Electrical and Electronic Engineering, Imperial College London, London, UK.

[3]Cancer Research UK Cambridge Research Institute, Cambridge, UK.

Grant sponsor: Engineering and Physical Sciences Research Council (EPSRC); Grant number: GR/S67135/01; Grant sponsor: Cancer Research UK; Grant number: C12A/A1209.

*Correspondence to: Franklyn Howe, Division of Cardiac and Vascular Sciences, St George's Hospital, University of London, Cranmer Terrace, London, SW17 0RE, UK. E-mail howefa@sgul.ac.uk

Received 17 July 2008; revised 9 October 2008; accepted 9 December 2008.

DOI 10.1002/mrm.21941

Published online in Wiley InterScience (www.interscience.wiley.com).

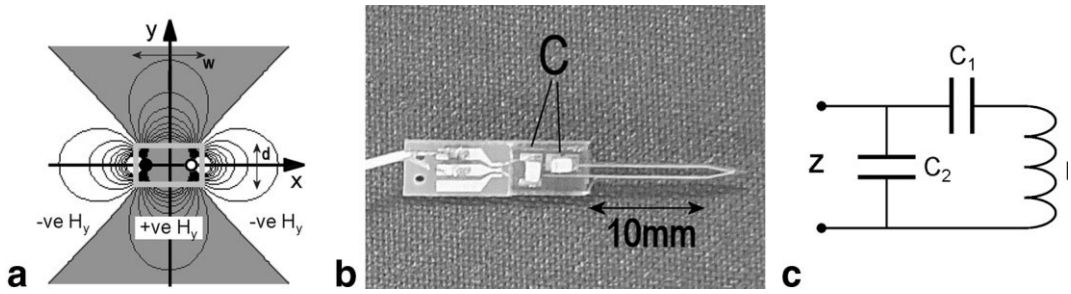

FIG. 1. **a:** Schematic cross-section of needle microcoil showing the H_y magnetic field isocontours of opposite polarity that are created from two parallel conductors. The rectangle depicts the encapsulated region of the coil with dimensions approximately 1.5 mm (width) × 1.0 mm (depth). **b:** Plastic needle microcoil showing the two 10-mm parallel conductors that form the active region of the coil and after the addition of tuning and matching capacitors (C) and coaxial cable. Note that the SU-8 encapsulation is transparent. **c:** Circuit diagram of the needle microcoil. Impedance Z is matched to 50 Ω capacitors required for a ^{31}P coil were typically C_1 = 253 pF and C_2 = 660 pF.

SRT Micro Céramique, France) and bond pads for connection to a small printed circuit board (PCB). Typical capacitance values for a plastic-shafted coil (which had a series resistance of ≈1Ω) operating at a frequency of 81 MHz were C_1 = 253 pF and C_2 = 660 pF, giving an effective capacitance of C_{Eff} = 183 pF. All-silicon coils used a similar effective capacitance at this frequency, and effective capacitances at 200 MHz were scaled according to the normal rules for inductor-capacitor (L-C) resonance. Balanced matching would certainly improve the signal-to-noise ratio (SNR), but would require additional components to be mounted on-chip, at the root of the needle. Given that space was at a premium in the wafer-scale fabrication process used, a simple unbalanced series-matching circuit was used, as shown in Fig. 1c.

In the hybrid design, conductors were first formed on 1.2-μm-thick layers of SiO_2, and then capped with a 500-μm-thick layer of SU-8 2050 resist (Chestech, UK). The lower shaft layer was then formed, by transferring the needle outline right through the Si wafer by deep reactive ion etching, a variant of plasma etching that can etch silicon with vertical side-walls (9). As a result, the conductors were embedded in a shaft measuring approximately 1.5 mm × 1.0 mm, as shown in Fig. 1. In the all-plastic design, conductors were formed on a 500-μm-thick SU-8 layer, which acted as the lower shaft layer. The upper half of the shaft was then formed in a further 500-μm-thick layer of SU-8. In this case, the constraints of processing necessitated a slightly wider shaft, so that the conductors lay 100 μm further from the surface. Finally, the entire plastic structure was detached by thermal shock from the Si substrate, which therefore acted only as a material support during processing.

Coils were tuned either to 81 MHz for ^{31}P spectroscopy at 4.7T (silicon-based and all-plastic needles) or 200 MHz for ^{1}H imaging (silicon-based needles), matched to 50 Ω, and connected to ultrathin coaxial cable via a small PCB that increased mechanical strength. Figure 1b shows an optical photograph of a needle coil with an all-plastic shaft, after addition of tuning and matching capacitors. The conductor layout may clearly be seen running along the length of the shaft.

NMR

^{31}P MRS and MRI were performed using a 4.7T small bore animal system (Varian, Inc., Palo Alto, CA, USA). For coil calibration in transmit/receive mode operation the needle coils were inserted full-length into small spherical bulbs containing either 10 μM $MnCl_2$-doped phosphate solution or 0.2% v/v Gd-diethylene triamine pentaacetic acid (DTPA)-doped water. Spectra were acquired unsaturated with either a 200-μs hard pulse (^{31}P MRS) or 5000-μs Gaussian pulse (^{1}H MRI) to find the signal maximum for each coil. Image sensitivity maps for a coil tuned to ^{1}H were acquired using a gradient echo sequence (TR = 200 ms, TE = 10 ms) with a Gaussian pulse to select a 1-mm slice orthogonal to the needle coil longitudinal axis with 1024 by 1024 resolution over a 40-mm field of view to give 0.04-mm in-plane resolution. Images were acquired with the needle coil parallel to the B_0 axis (the orientation for ^{31}P MRS acquisition) as well as with the coil orthogonal to B_0.

All animal experiments were performed in accordance with the local ethical review panel and the UK Home Office Animals Scientific Procedures Act of 1986. Wistar Furth rats (N = 3) were used for in vivo measurements with nonrecovery from anesthetic after the experiment. Under general anesthesia, a flap of skin was removed from over the thigh muscle to enable a needle microcoil to be inserted parallel to the muscle fibers and with minimal muscle tissue damage. The rat was then laid prone in the magnet bore within a whole-body imaging coil with heated air flow to maintain body temperature. Gradient echo images were obtained to confirm the coil position within the muscle bulk. A point-resolved spectroscopy sequence (PRESS) localization sequence (10) was used to shim over the region of muscle containing the needle coil. Using the phantom calibration pulse power for maximum signal, ^{31}P spectra were acquired in vivo from rat thigh muscle with TR = 2500 ms for the silicon substrate needle coil, and TR = 2000 ms for the plastic substrate needle coil in blocks of 256 transients for 60 min.

^{31}P spectra were analyzed using the VARPRO time domain method as implemented in the jMRUI package (http://www.mrui.uab.es/mrui/mrui_Overview.shtml) with prior knowledge as previously described (11). In practice, the linewidths of the inorganic phosphate (Pi), phosphocreatine (PCr) peaks, and individual components of the adenosine triphosphate (ATP) resonances were dominated by the field inhomogeneity and so all were set equal.

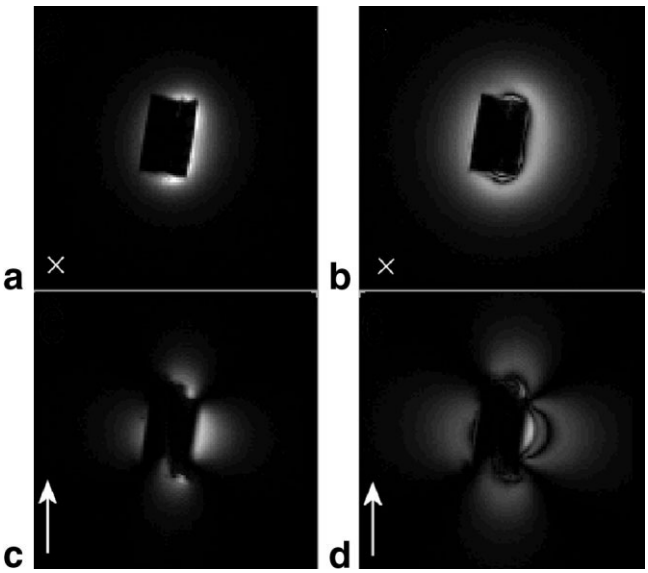

FIG. 2. Gradient echo images acquired transverse to the longitudinal axis of a ^{1}H tuned needle microcoil inserted into a bulb containing Gd-DTPA-doped water. The central signal void is the SU-8 encapsulation with the 1-mm separation of the parallel conductors across the wider part of the cross-section. The arrows and cross indicate the direction of the B_0 field. Excitation pulse power was set at 12 dB below that giving maximum pulse-acquire signal for (**a**) and (**c**) and set for a maximum pulse-acquire signal in (**b**) and (**d**). Note that the slight left-right asymmetry of the signal intensity is due to a small difference in the thickness of the encapsulation above and below the conductors. In (c) and (d) there are also small image distortions due to greater susceptibility artifacts close to the coil surface for the coil orientation used for these images.

RESULTS

At the frequencies used here, both types of coil had similar electrical performance. Coil inductance was 21 nH, and coil Q was typically 11 for ^{31}P and 25 for ^{1}H coils as measured with an Agilent E5061A network analyzer. However, all-plastic coils had higher Q-factors at higher frequencies (e.g., 200 MHz as required for ^{1}H MRS at 4.7T). Coil Q measured in saline solution to simulate maximum loading was not different to an unloaded coil, indicating that the coil is the dominant noise source. ^{1}H images that depict the coil sensitivity distribution of the coil are shown for two orientations and two excitation-pulse power levels in Fig. 2. For an excitation-pulse power 12 dB below that giving maximum nonlocalized signal, the flip angle at the coil surface is approximately 90 degrees, as shown by there being a single maximum signal adjacent to the coil substrate (Fig. 2a and c). With the coil oriented perpendicular to the B_0 field, only the B_y component of the radiofrequency pulse produces a signal, hence a quadrupolar sensitivity distribution (Fig. 2c and d) similar to that depicted in Fig. 1 is observed. Defining the maximum total signal in a nonlocalized pulse-acquire measurement obtained with the coil parallel to B_0 (Fig. 2b) as 100%, then at the –12-dB excitation pulse power level the total signal was 50% (Fig. 2a), for the perpendicular orientation the maximum signal intensity was 53% (Fig. 2d), and at the –12-dB pulse power level the total signal was 37% (Fig. 2c).

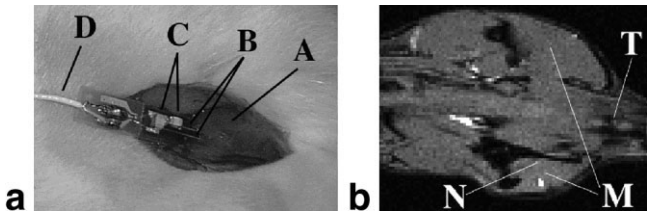

FIG. 3. **a:** Needle microcoil inserted into rat thigh muscle along the muscle fiber direction. A = thigh muscle with overlying skin removed, B = needle microcoil conductors, C = tune and match capacitors, D = coaxial cable to spectrometer. **b:** Coronal MR image through a prone rat. M = thigh muscles, T = tail, N = signal void of needle coil track.

Figure 3a shows the needle microcoil inserted into rat thigh muscle. Ideally the coil longitudinal axis would be aligned parallel to the B_0 field, but in practice this is not possible due to limitations in positioning the rat within the experimental setup. Figure 3b shows a coronal MR image acquired with the volume coil that illustrates the signal void of the microcoil track within the muscle. We estimate that the coil axis lies within 20° to the B_0 axis in all in vivo experiments, hence the sensitive region of tissue from which the ^{31}P spectra are acquired is most like that depicted in Fig. 2b.

Figure 4 shows a ^{31}P spectrum obtained in 11 min (4 blocks of 256 transients), which had a SNR of 10.4 (equivalent to an SNR of 3.1 per $\text{min}^{1/2}$ of total acquisition time) for the PCr in the spectrum with the lowest linewidth of 19 Hz (as calculated by VARPRO prior to line-broadening). On average ($N = 3$), the PCr linewidth was 31 ± 12 Hz; the PCr SNR (with 15-Hz line-broadening) was 2.2 ± 0.5 per $\text{min}^{1/2}$ of total acquisition time; the PCr/ATP ratio was 3.5 ± 0.5; and the PCr amplitude decreased by 22 ± 14% over 60 min. Inorganic phosphate was only observable in one block of 1024 transients and enabled an intracellular pH (pH_i) of 6.6 to be estimated. Comparison of the PCr SNR between needle-coil types was made after normalizing for the linewidth (i.e., by multiplying by the VARPRO-determined linewidth in Hz) to account for shim variation and

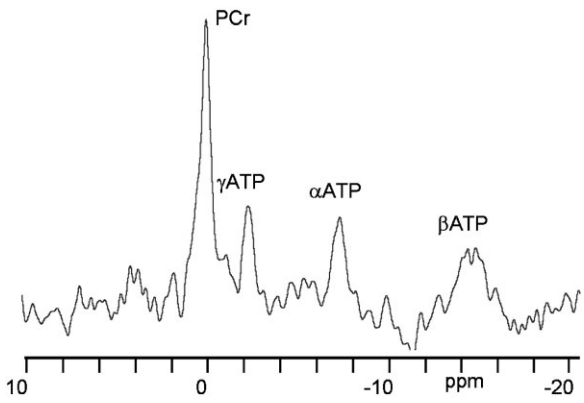

FIG. 4. In vivo ^{31}P spectrum acquired at 80 MHz from rat thigh muscle with a needle microcoil using TR = 2500 ms and 256 signal averages, and processed with 15-Hz line-broadening. SNR of PCr = 10.4.

was 60 per $min^{1/2}$ Hz (silicon-based coil) and 78 per $min^{1/2}$ Hz (mean from two all-plastic coils).

DISCUSSION

We have demonstrated the feasibility of obtaining in vivo ^{31}P spectra and ^{1}H images using a needle microcoil design that can be batch manufactured and inserted into tissue. The PCr/ATP peak area ratio obtained is similar to that expected for rat muscle from in vivo studies (12,13). Not surprisingly with such an invasive MRS approach, there is evidence of ischemia due to tissue damage, as shown by the low pH_i and the decrease in PCr over time. Nevertheless, a role for the needle coil can be envisaged in the acquisition of tumor spectra during interventional surgery, or in obtaining spectra or images from the walls of large blood vessels. With the coil used for both transmission and reception, there is an orientation-dependent sensitive volume of tissue, with maximum signal received for the coil aligned along the B_0 axis. However, as long as the B_0 field lies within the plane of the two parallel conductors it is possible to obtain a signal for the coil at any angle, with a variation in total signal intensity of approximately a factor of 2.

The linewidth-corrected data show a similar SNR of the PCr peak for the silicon-based and all-plastic coils, which is in keeping with their similar Q as measured on the bench. The variation in PCr linewidth between the three experiments may arise from shimming an encompassing large voxel rather than the sensitive volume of the needle-coil and may be the factor reducing the SNR from optimum. Shimming over the coil-sensitive region using the coil itself if tuned to ^{1}H may therefore improve the SNR. For ^{1}H MRS at 1.5T (64 MHz) the proton concentrations for the CH_3 moieties commonly observed in tumors (e.g., cholines, creatine, and lactate) are similar to that for the phosphorus concentration of PCr in muscle. Hence the SNR observed in Fig. 4 may be realizable in a clinical interventional MRI system for ^{1}H MRS for a similar acquisition time. With this needle microcoil design the Q is very low compared to the 50 to 100 typical of small surface coils used in animal studies. A further increase in Q is still feasible with the current design and a further improvement in SNR is likely to be obtained by the use of adiabatic pulses (14). Hence it is feasible that useful spectra may be obtainable in a clinical setup from tissue within a few minutes. We now aim to improve the current design in a number of directions with the aim of increasing its Q, increasing both its mechanical and electrical robustness, and further integrating the components needed to make them compatible with MR systems.

ACKNOWLEDGMENTS

Coil development was funded by the Engineering and Physical Sciences Research Council (EPSRC), and MR facilities were funded by Cancer Research UK.

REFERENCES

1. Peck TL, Magin RL, Kruse J, Feng M. NMR microspectroscopy on 100-μm planar RF coils fabricated on gallium arsenide substrates. IEEE Trans Biomed Eng 1994;41:706–709.
2. Neagu CR, Jansen HV, Smith A, Gardeniers JGE, Elwenspoek MC. Characterization of a planar microcoil for implantable microsystems. Sens Actuators A Phys 1997;62:599–611.
3. Dechow J, Forchel A, Lanz T, Haase A. Fabrication of NMR- microsensors for nanoliter sample volumes. Microelectron Eng 2000;53:517–519.
4. Woytaskik M, Ginefri J-C, Raynaud J-S, Poirier-Wuinot M, Dufour-Gergam E, Grandchamp J-P, Girard O, Robert P, Gilles J-P, Martincic E, Darasse L. Characterisation of flexible RF microcoils dedicated to local MRI. Microsystems Technol 2007;13:1575–1580.
5. Berry L. Renaud L, Kleimann P, Morin P, Armenean M, Saint-Jalmes H. Development of implantable detection microcoils for minimally invasive NMR spectroscopy. Sens Actuators A Phys 2001;93:214–218.
6. Syms RRA, Ahmad MM, Young IR, Gilderdale DJ, Collins DJ. Micro-engineered needle micro-coils for magnetic resonance spectroscopy. J Micromech Microeng 2006;16:2755–2764.
7. Ahmad MM, Syms RRA, Howe FA, Rodrigues LM, Young IR. Development of all-plastic needle coils made using silicon technology. In: Proceedings of the 15th Annual Meeting of ISMRM, Berlin, Germany, 2007 (Abstract 324).
8. Lorenz H, Despont M, Fahrni N, LaBianca N, Renaud P, Vettinger P. SU-8: a low-cost negative resist for MEMS. J Micromech Microeng 1997;7:121–124.
9. Hynes AM, Ashraf H, Bhardwaj JK, Hopkins J, Johnston I, Shepherd JN. Recent advances in silicon etching for MEMS using the ASE™ process. Sens Actuators A Phys 1999;74:13–17.
10. Bottomley PA. Human in vivo NMR spectroscopy in diagnostic medicine: clinical tool or research probe? Radiology 1989;170:1–15.
11. Stubbs M, van den Boogaart A, Bashford CL, Miranda PMC, Rodrigues LM, Howe FA, Griffiths JR. ^{31}P-magnetic resonance spectroscopy studies of nucleated and non-nucleated erythrocytes; time domain data analysis (VARPRO) incorporating prior knowledge can give information on the binding of ADP. Biochim Biophys Acta 1996;1291:143–148.
12. Howe FA, Stubbs M, Rodrigues LM, Griffiths JR. An assessment of artefacts in localized and non-localized ^{31}P MRS studies of phosphate metabolites and pH in rat tumours. NMR Biomed 1993;6:43–52.
13. Morikawa S, Kido C, Inubushi T. Observation of rat hind limb skeletal muscle during arterial occlusion and reperfusion by ^{31}P MRS and ^{1}H MRI. Magn Reson Imaging 1991;9:269–274.
14. Garwood M, DeLaBarre L. The return of the frequency sweep: designing adiabatic pulses for contemporary NMR. J Magn Reson 2001;153:155–177.